Aero-Thermal Heating of Conical Leading Edges on Aircraft Noses Using CFD

Brandon Voll
Wilson Ezequelle

Computational Fluid Dynamics
Department of Mechanical Engineering
School of Engineering
The University of Vermont

October 27, 2021

Abstract

The objective of this computational fluid dynamics (CFD) study is to research the aero-thermal heating of nose-cone leading edges of varying shapes. The thermal heating will be compared to the X-15 aircraft which the model for the computational study was based upon. Understanding the thermal conditions of leading edges on aircraft in the supersonic and hypersonic regime is extremely important as heating of the surface becomes extreme at these high speeds. Material and shapes of the leading edges and even the body of the aircraft must be done carefully to ensure that there will be no damage to the aircraft during flight. Two CFD studies were carried out on the X-15 nose cone which included a ramp up in Mach from 0 to 7 as well as a constant Mach transient study held for 150 seconds or greater. These conditions were also carried out for two similar nose cone shapes including one with a blunt shape and one with a diamond shape for comparison. The results of these simulations show that at hypersonic speeds, the blunt nose cone experiences a lower stagnation temperature than the X-15 nose cone model. This is important in order to ensure that the maximum temperature does not exceed the allowable temperatures of the materials or components housed in the nose cone.

Nomenclature

A = Area $[m^2]$

C_f = Skin Friction Drag Coefficient

D = Drag $[N]$

M = Mach Number

Q = Heat Transfer per Unit Time $[W]$

T = Temperature $[K]$

U_0 = Velocity at Infinity $[\frac{m}{s}]$

dT = Temperature Difference Between the Surface and the Fluid $[K]$

h = Enthalpy $[J]$

h_c = Convective Heat Transfer Coefficient $[\frac{W}{m^2K}]$

k = Thermal Conductivity $[\frac{W}{mk}]$

r = Radius of Cross-Section of Body $[m]$

u = Velocity in Boundary Layer$[\frac{m}{s}]$

x = Material Thickness $[m]$

y = Distance Normal to Surface $[m]$

γ = Specific Heat Ratio

ρ = Density $[\frac{kg}{m^3}]$

ξ = Distance Measured Parallel to Axis of Body From Stagnation Point $[m]$

Contents

1 Motivation and Background 5

2 Physical Model 7

2.1 Assumptions 11

3 Numerical Models 13

4 Boundary Conditions 14

5 Mesh and Grid Study 17

6 Convergence 24

7 Results and Discussion 26

7.1 Ramp Up Mach Number 26

7.2 Constant Mach Number 31

8 Conclusions 36

1 Motivation and Background

The heating of a solid during high speed flow is a common engineering problem that must be examined during the design of many aircraft's leading edges. The nose cone of an aircraft can reach incredible temperatures and even failure if the proper material and cooling methods are not selected. In order to do this, the maximum temperature that different locations may experience and how the heat diffuses through the solid must be known for different conditions. This problem becomes even more prevalent when dealing with hypersonic flow.

It seems to almost be fundamental to think that a sharp, sleek looking body is meant to go fast. Even at an early age, most individuals associate this shape with speed. Manufacturers of consumer products take advantage of this and design products to look fast even if they are not relatively fast. But, even though this is sometimes exploited as a gimmick, there are facts behind the thought that make it true in some cases.

Since the advent of mechanical devices for travel, making these devices faster is one of the most sought after components of advancement. This is one of the most important components of aircraft design. Nose-cones are the front-most point of an aircraft and thus take the brunt of the flow, and dictate how the flow will begin to move around the aircraft. For sub-sonic aircraft, typically nose-cones are blunted because the flow has time to move around the aircraft and this allows drag to be minimized. For supersonic flow, is is ideal to have as sharp a leading edge as possible. This is because the flow no longer has time to move before reaching the surface, which is why a shock is formed. Hypersonic flow takes on new characteristics where the material that is used for the leading edge needs to withstand high temperatures, so it is again useful to have a blunt leading edge as this has a larger volume to dissipate heat and creates a detached bow shock.

Some examples of each of these cases follow. A subsonic aircraft would be passenger jets such as a Boeing 747. This aircraft has a very large nose area and is quite blunt. This is easier to manufacture, allows for more space inside of the aircraft, and reduces drag. A supersonic aircraft

example is the Concorde. The Concorde had a sharp nose-cone because it traveled as supersonic speeds. This reduced drag but was harder to manufacture, and made landing difficult because a sharp nose requires a longer nose section in general. An example of a hypersonic vehicle would of course be the X-15. The X-15 had a spherical blunt shaped leading edge which allowed for more heating due to its thermal mass and shock creation characteristics, which were necessary at hypersonic speeds with the current material technology.

2 Physical Model

The physical model for this simulation is based off of the nose-cone for the X-15 experimental aircraft flown by NASA. The X-15 was produced as an experimental aircraft to study the hypersonic regime. The data that was collected by the X-15 was imperative to the success of many NASA projects including Apollo which was in development while the X-15 was being used.

The nose-cone for the X-15 was important not only because it was the leading edge of the aircraft and would take a brunt of the heating, but also because it housed an instrument cluster which was used for navigation. The entire nose section was approximately 0.43 meters long with a radius at the back of 0.175 meters. The extreme tip of the nose was a sphere of radius 0.0825 meters and was constructed of Inconel X, a highly heat resistant material [7].

For the purposes of this simulation, the nose section was simplified to be one solid piece of Inconel X. The actual nose of the X-15 had various cavities which housed instruments as well as cooling veins which pumped a fluid solution [7].

AutoCAD was used to create this model, along with the fluid domain which would surround the nose. The model which was used to simulate the X-15 nose can be seen in Figure 1.

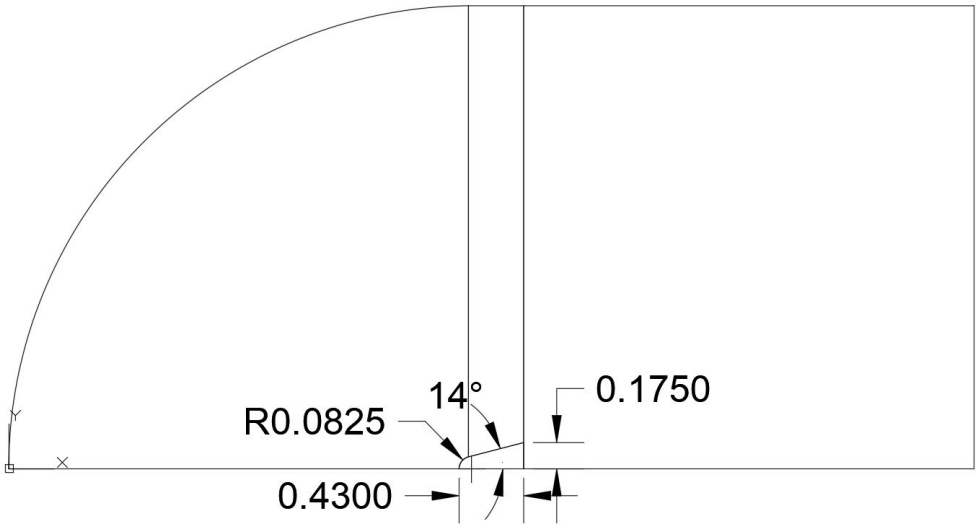

Figure 1: AutoCAD model depicting the X-15 nose section made of Inconel X.

The objective of this work was to compare this model to other similar models. These models had similar dimensions but varying tip geometries. These geometries included a blunt geometry and a diamond geometry. The models for these geometries can be seen in Figure 2 and Figure 3, respectively.

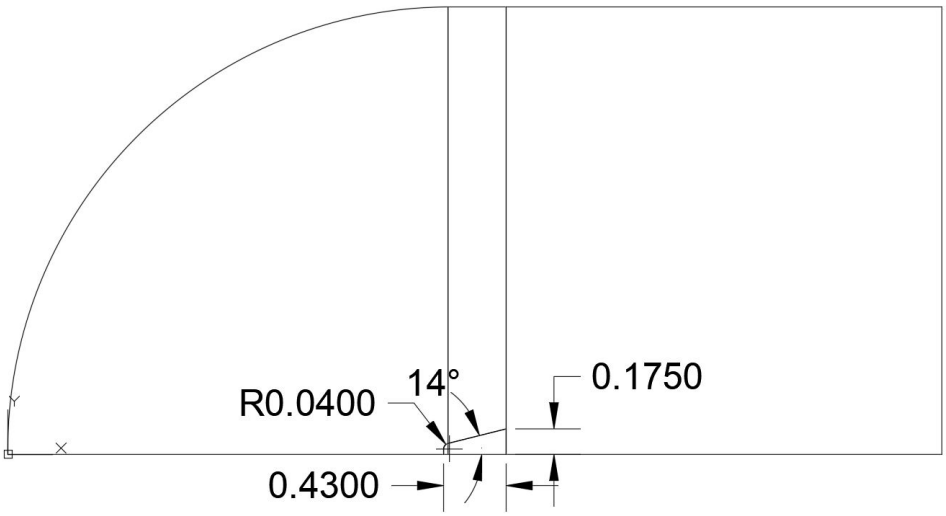

Figure 2: AutoCAD model depicting a blunt shaped nose-cone.

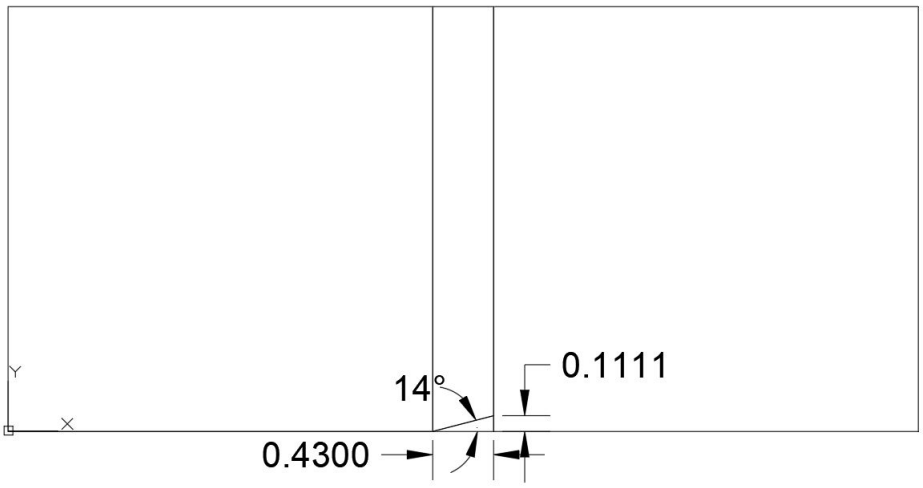

Figure 3: AutoCAD model depicting a diamond shaped nose-cone.

In the subsonic regime, flow moving over a body does not vary in density and no chemical reactions occur. Essentially, "information" travels upstream of the flow which tells the upstream flow that it needs to turn to get around an object impinging on the flow. When a flow reaches the

transonic regime and further, this information is no longer able to travel upstream and therefore the flow does not know that is needs to turn to avoid an object. This is the essential idea behind compressible flow. To compensate for this lack of information, a shock wave is formed which compresses the flow and decreases the velocity of the flow. For any blunt shaped body, this causes a normal shock, which is perpendicular to the flow at the stagnation point and slowly arcs outward following the curve of the object. For a pointed object, the shock is able to attach to the tip of the object which creates an oblique shock. What is important to note is that the oblique shock is still governed by the relations used for the normal shock, as only the normal portion of the flow is important when carrying out calculations for an oblique shock.

In the subsonic regime, the heat transfer to the surface is characterized by convection as well as the skin friction which will occur from the drag imparted by the flow. The convection in the subsonic regime can be characterized by Newton's Law of Cooling which can be seen in Equation 1 [3].

$$Q = h_c A dT \tag{1}$$

The conduction of the solid can be characterized by Fourier's Law. This can be seen in Equation 2 [2].

$$Q = \frac{k}{x} A dT \tag{2}$$

When moving into the supersonic and hypersonic regime, the same conditions apply for the heat transfer but the properties in front of the leading edge will change. As stated earlier, the density will change but more importantly for this case the temperature will also change. For a normal shock in a calorically perfect ideal gas, the temperature is a function of the specific heat ratio (1.4 for air) and the Mach number. The temperature behind the shock can be found using Equation 3 [1].

$$T_2 = T_1[1 + \frac{2\gamma}{\gamma+1}(M_1^2 - 1)][\frac{2 + (\gamma-1)M_1^2}{(\gamma+1)M_1^2}] \tag{3}$$

It is important to note that air dissociation is not taken into account in this simulation. The oxygen in air begins to dissociate at moderate pressures at a temperature of about 2000K [5]. The data which will be analyzed shows temperatures which could enter into the dissociation regime. The CFD model assumes that no dissociation occurs so it is important to note that this is a simplification in the simulation. If dissociation was to be taken into account the temperature behind the shock would be a function of pressure and enthalpy. The enthalpy can be found using Equation 4 and the temperature can than be found iteratively [1].

$$h_2 = h_1 + \frac{u_1^2}{2}[1 - (\frac{\rho_1}{\rho_2})^2] \tag{4}$$

The final addition of heat that will be incident on the surface is from skin friction. Skin friction is a product of drag on the surface. Drag is characterized in Equation 5 [8].

$$D = 2\pi\rho \int_0^\infty u(U_0 - u)ydy \tag{5}$$

If τ_0 is the local skin friction coefficient at a point on the surface, than the skin friction drag coefficient on the body can by found using Equation 6 [8].

$$C_f = \frac{2}{A}\int_0^l \frac{\tau_0}{\rho U_0^2} 2\pi r d\xi \tag{6}$$

2.1 Assumptions

- The nose-cone in the CFD model is one solid piece of Inconel X, whereas the actual X-15 nose-cone has instrumentation within it as well as cooling veins which are used to pump

liquid nitrogen.

- The flight path of the simulation is at one elevation (sea-level) whereas the actual X-15 would undergo a complicated flight trajectory which is unable to be matched in this case.
- The model for the simulation is of the nose-cone only, therefore there will be an expansion wave at the rear of the model. This would not be the case for a real aircraft.
- The dissociation of molecules is not taken into account for this situation, even though it is possible that dissociation did take place in the actual flights.

Because of these assumptions and simplifications, it is understood that the work carried out in this report is not representative of the actual physical phenomena which would be experienced by the X-15 or any other aircraft performing under the specified circumstances.

3 Numerical Models

The simulations deal with compressible flow, therefore the density-based solver must be used with absolute velocity formulation. The simulations are also transient in axisymmetric 2D space. Models:

- Viscous laminar
- Energy equation on

The fluid air properties:

- Ideal gas density model
- Thermal conductivity = .0242 $W/m-K$
- Viscosity = $1.7894x10^{-5}kg/m-s$
- Molecular weight = 28.966 $kg/kmol$

Solid inconel properties [6]:

- Density = 828 kg/m^3
- Specific heat = 431 $J/kg-K$
- Thermal conductivity = 12 $W/m-K$

Methods:

- Formulation - implicit
- Flux type - Roe-FDS

- Gradient - least squares cell based
- Flow - first order upwind
- Transient formulation - first order implicit

4 Boundary Conditions

A pressure far field boundary condition was used in two different ways. It was used for a transient simulation with a constant Mach number of 6.04 and also with a user defined function for the Mach number that increased the Mach number from .05 to 7.13 over a period of 12 seconds. For both of these cases, the Gauge pressure was 101325 Pa and the flow was strictly axial with no radial component. An axis boundary condition runs along the entirety of the domain at y=0. Both of these boundary conditions can be seen below in Figure 4.

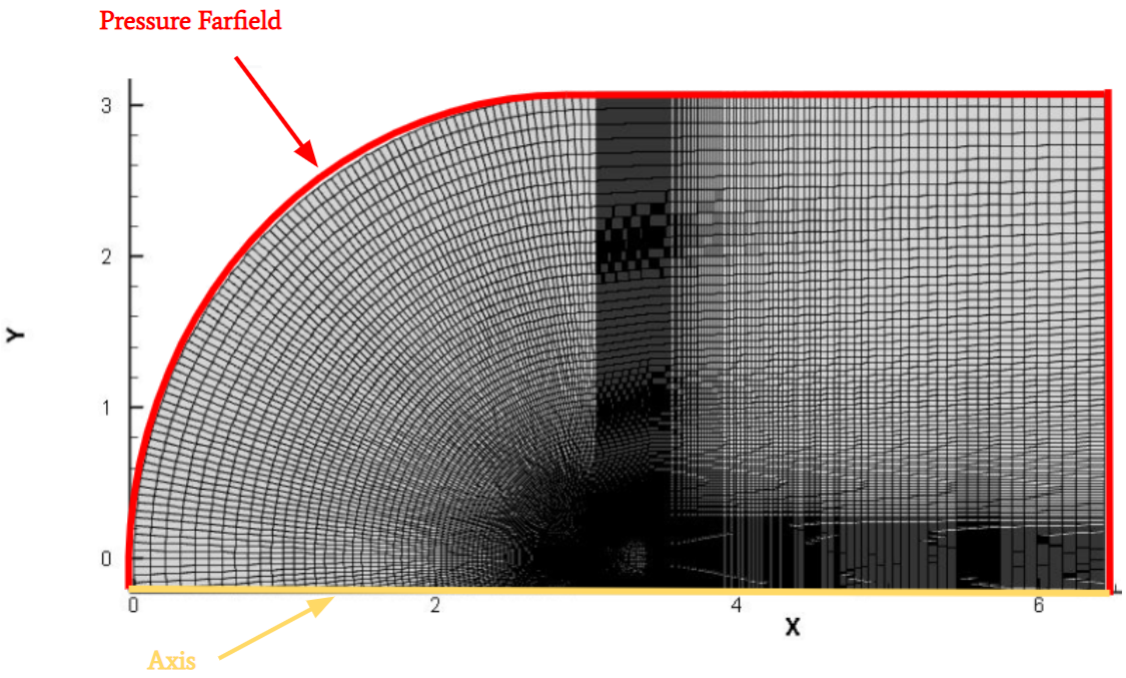

Figure 4: Exterior Boundary Conditions.

The solid and the fluid are meshed separately so they must interact through a coupled mesh interface between the solid wall interface and fluid wall interface. This is necessary in order to be able to examine the thermal reaction in the solid separately. These interfaces can be visualized in Figure 5 below.

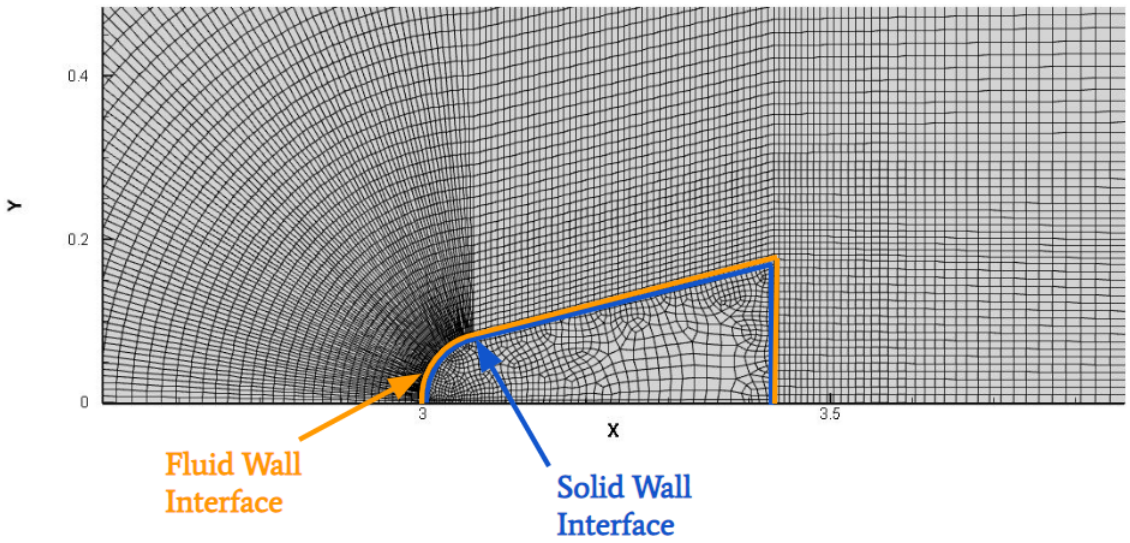

Figure 5: Solid Boundary Conditions.

The operating pressure was set to 0 Pa. Two different transient simulations were completed for each of the geometries. The first being the previously mentioned Mach number ramp up in which 240 time steps of .05 seconds were solved for. The constant Mach case consisted of 150 times steps of 1 second each at a Mach number of 6.04.

5 Mesh and Grid Study

A mesh sensitivity study was carried out to determine the optimal number of finite volumes needed to produce reliable results while also maintaining fast calculation speeds by minimizing the finite volume count. As thermal conditions are the parameters of interest for this study, temperature and drag were used as monitors to converge on a solution. For this study there are also two parts in the model, the fluid and the solid. The fluid will be analyzed first. An area-weighted average of static temperature was created 0.01 meters in front of the solid with a line 0.15 meters tall. A steady state Fluent case was carried out at Mach 2 until convergence with a varying number of finite volumes. Figure 6 shows how the temperature reached a value of about 368K at this point with just over 20000 finite volumes.

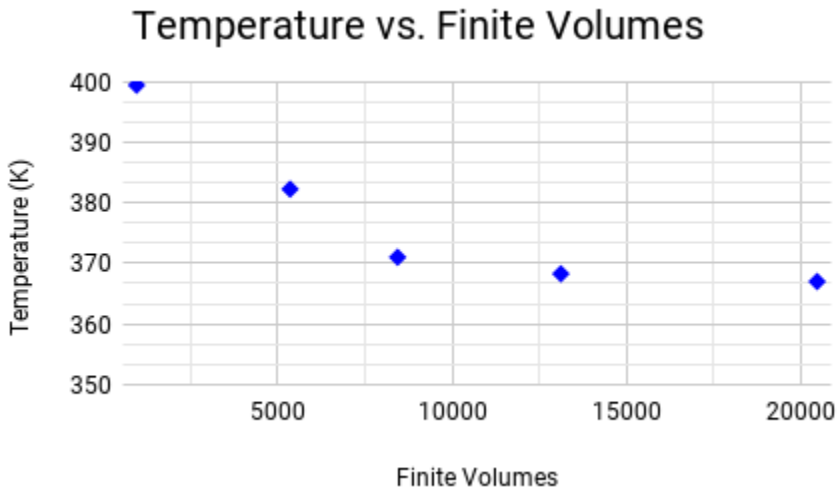

Figure 6: Mesh Study on X-15 nose cone model showing how stagnation point temperature varies with the number of finite volumes in the fluid.

Figure 7 shows the percent change of values from Figure 6. It can be seen that the percent change reaches a value below 1%.

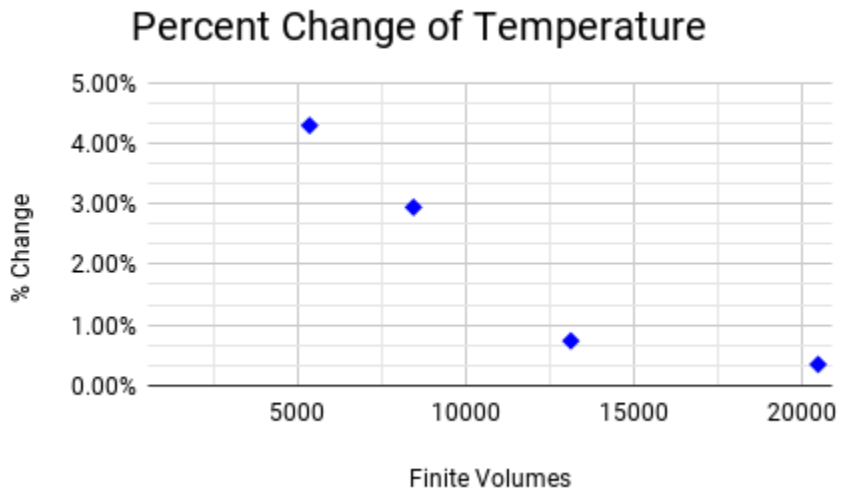

Figure 7: Mesh Study on X-15 nose cone model showing how the percent change of stagnation point temperature varies with the number of finite volumes in the fluid.

An area-weighted average monitor for drag was created on the interface of the fluid and solid, in other words the solid wall. The drag was measured in Newtons and Figure 8 shows the relationship between drag and the number of finite volumes.

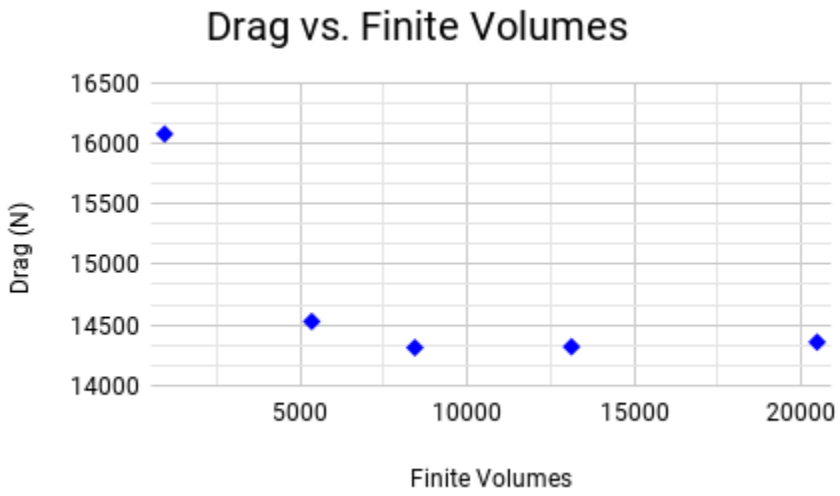

Figure 8: Mesh Study on X-15 nose cone model showing how drag varies with the number of finite volumes in the fluid.

Figure 9 shows the percent change in drag of the values of drag from Figure 8. The values can be seen to drop below 1% as well.

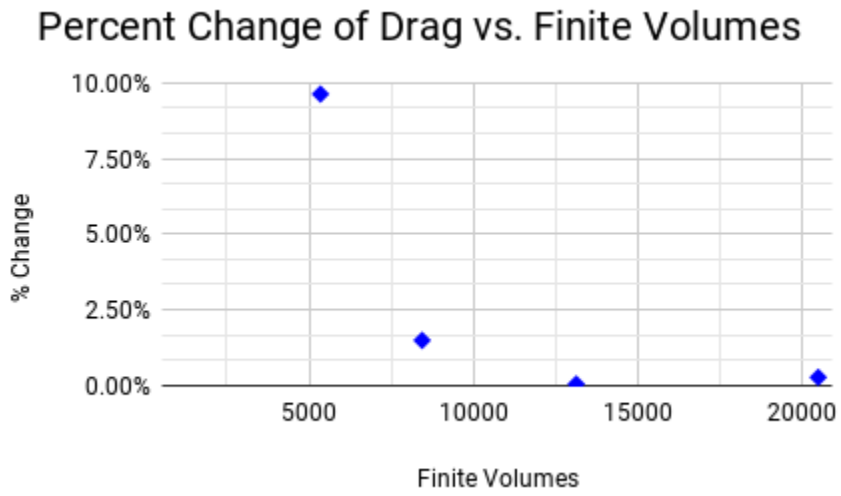

Figure 9: Mesh Study on X-15 nose cone model showing how the percent change of drag varies with the number of finite volumes in the fluid.

From the two previous monitors, it was determined that a mesh with about 20,000 finite volumes would be sufficient for the fluid region.

The solid region of the model was expected to go through pure diffusion. Pure diffusion does not require many finite volumes in Fluent, therefore a lower range of finite volumes was used for this portion of the sensitivity study. Figure 10 used a range from about 300 to just over 2000 finite volumes. An area-weighted average monitor of temperature was created using a vertical line 0.03 meters into the solid from the stagnation point and extending to the surface of the solid.

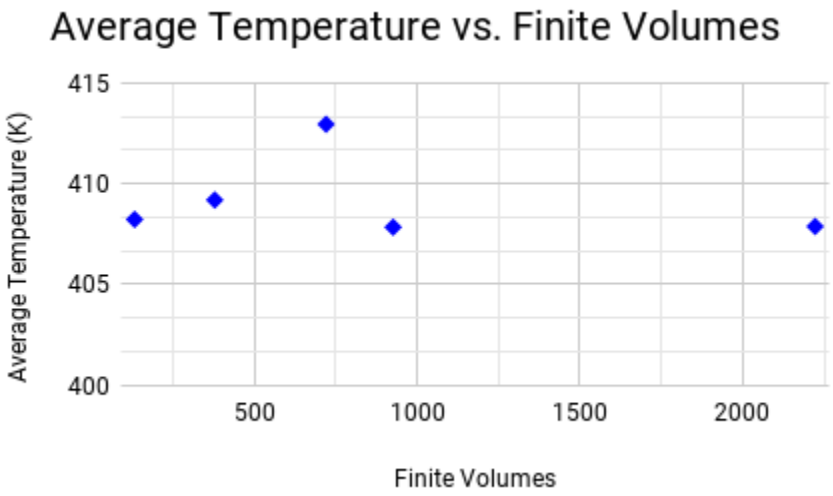

Figure 10: Mesh Study on X-15 nose cone model showing how stagnation point temperature varies with the number of finite volumes in the solid.

Figure 11 shows the percent change of temperature within the solid from Figure 10. It can be seen that all of the changes are very low, with the highest percent change only being 1.25%.

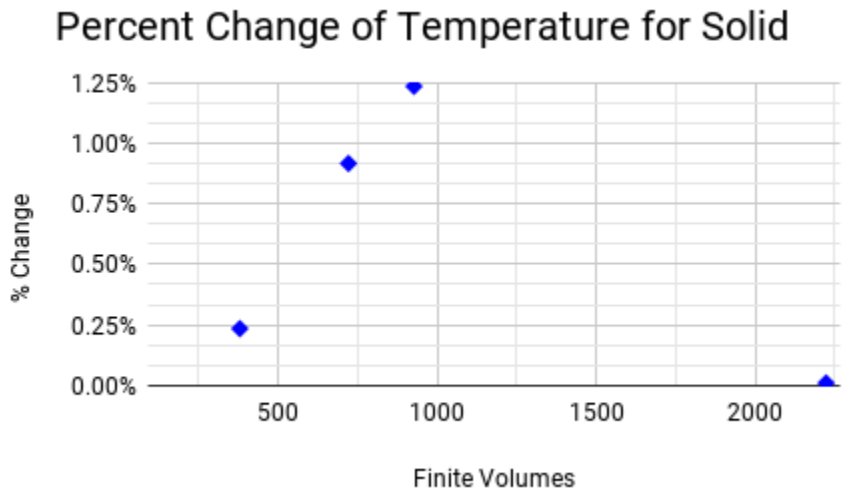

Figure 11: Mesh Study on X-15 nose cone model showing how the percent change of stagnation point temperature varies with the number of finite volumes in the solid.

From these results, it was determined that 1000 finite volumes would be sufficient within the solid.

Figures 12 and 13 show the mesh for the X-15 nose cone model. Similar meshes were created for the diamond and blunt model cases.

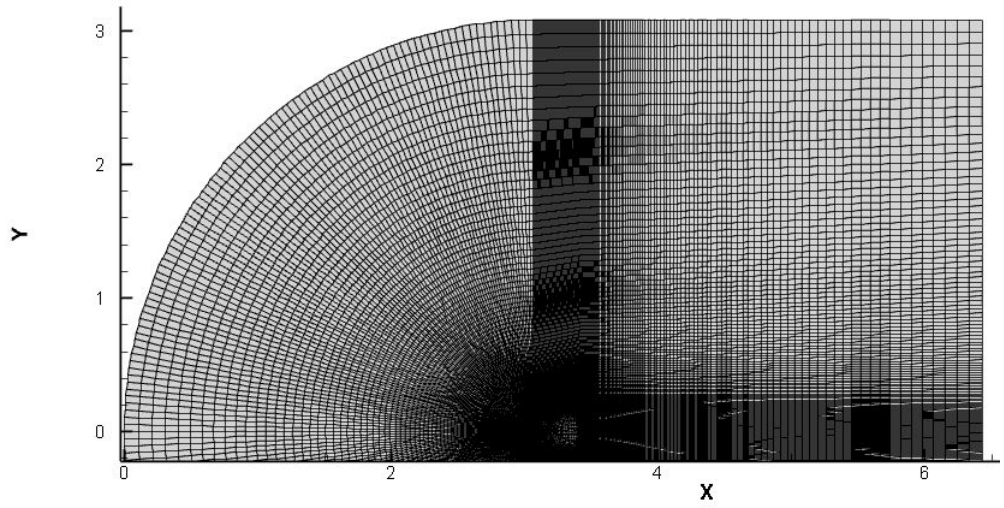

Figure 12: Mesh of the X-15 nose cone model with 20,480 finite volumes.

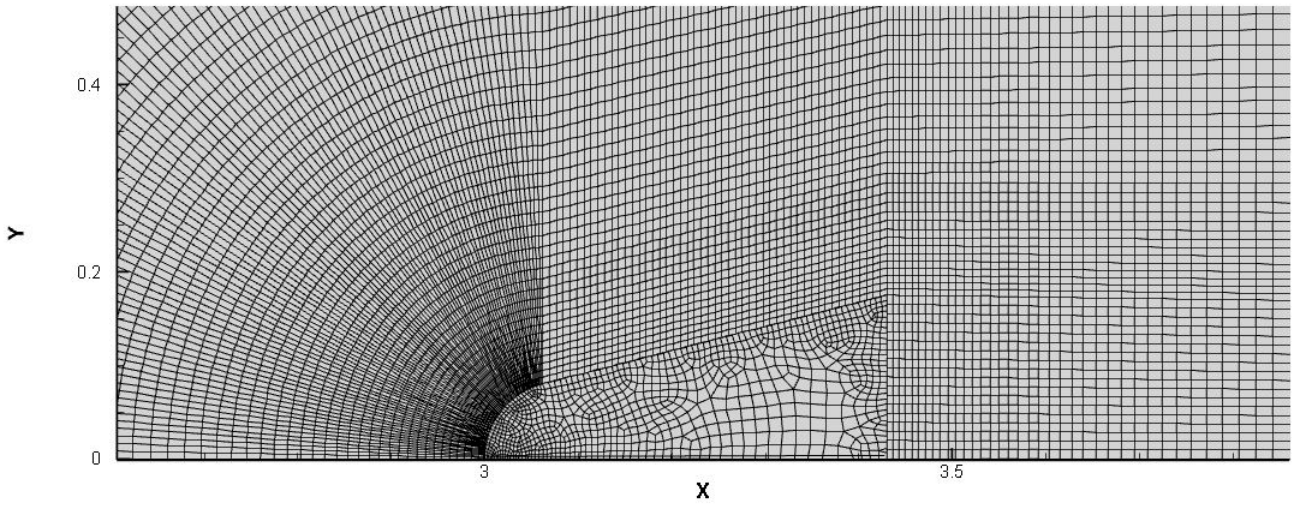

Figure 13: Close up view of the solid mesh within the X-15 nose cone model with about 1,000 finite volumes in the solid.

6 Convergence

There were two main cases that were performed for each of the models. This included a ramp up case where the Mach number was increased from 0 to 7 as well as a constant Mach case where the Mach number was 6.04. The reason for this will be explained in a later section.

Figure 14 shows typical residuals for a time step in the Mach ramp up case. Over the course of the case, the number of iterations needed to be changed quite a bit due to the large difference in initial and final Mach number. Some residuals converged nicely and quickly in as little as 2000 iterations, while others needed up to 4500 iterations and still did not quite reach the same point as the lower residuals. These points seemed to coincide with both the transonic regime and a certain point in the flow time where the Mach number became so high that a large number of iterations did not result in the same residuals.

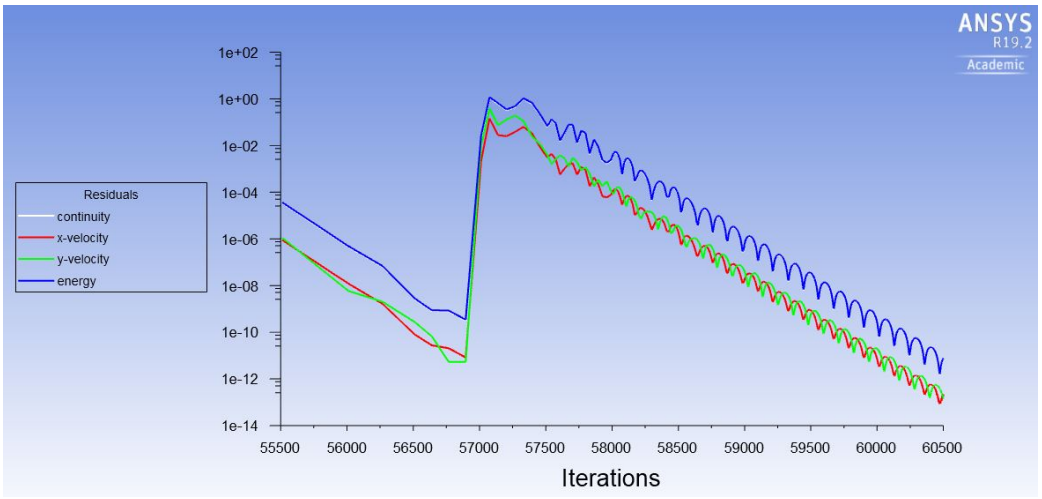

Figure 14: Example of residuals in the ramp up Mach case using the X-15 nose cone shaped model.

Figure 15 shows typical residuals for the constant Mach case. Two time steps are shown here which include the first time step where the residuals converged on a value and the following time step where the residuals did not jump back up. This is because with the constant Mach number, not

much was changing in the flow or solid. Once convergence was reached, it took very few iterations to reach convergence again.

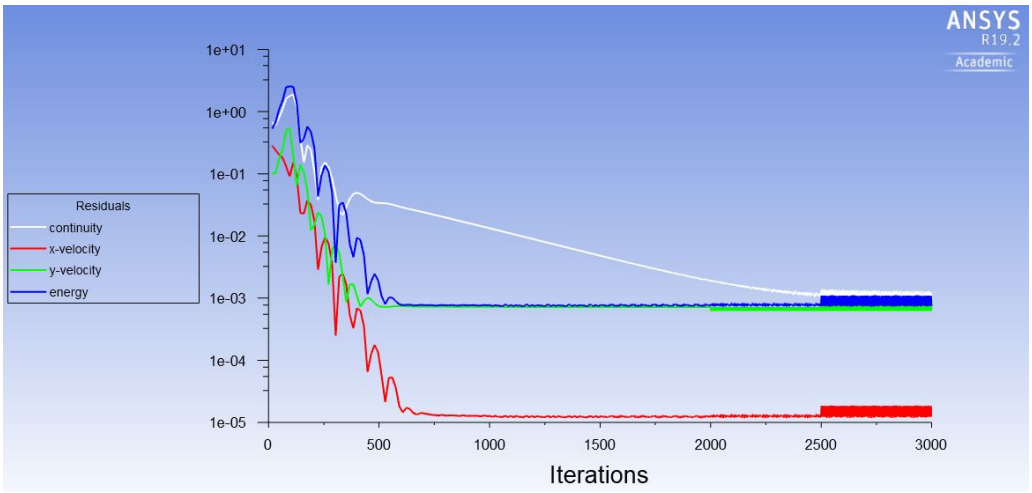

Figure 15: Example of residuals in the constant Mach case using the X-15 nose cone shaped model.

The residuals shown in Figure 14 and Figure 15 were both for the X-15 nose cone model. The diamond and blunt models showed similar behaviour so they are not shown for the interest of space.

7 Results and Discussion

7.1 Ramp Up Mach Number

As the Mach number increases linearly, the drag on each of the different nose cones will also increase. The blunt nose cone experiences the greatest drag force as it creates the greatest obstruction to the flow. Both the X-15 model and the blunt nose model increase at a more rapid rate than the diamond nose cone and do not follow a linear increase. These trends can be seen in Figure 16 below.

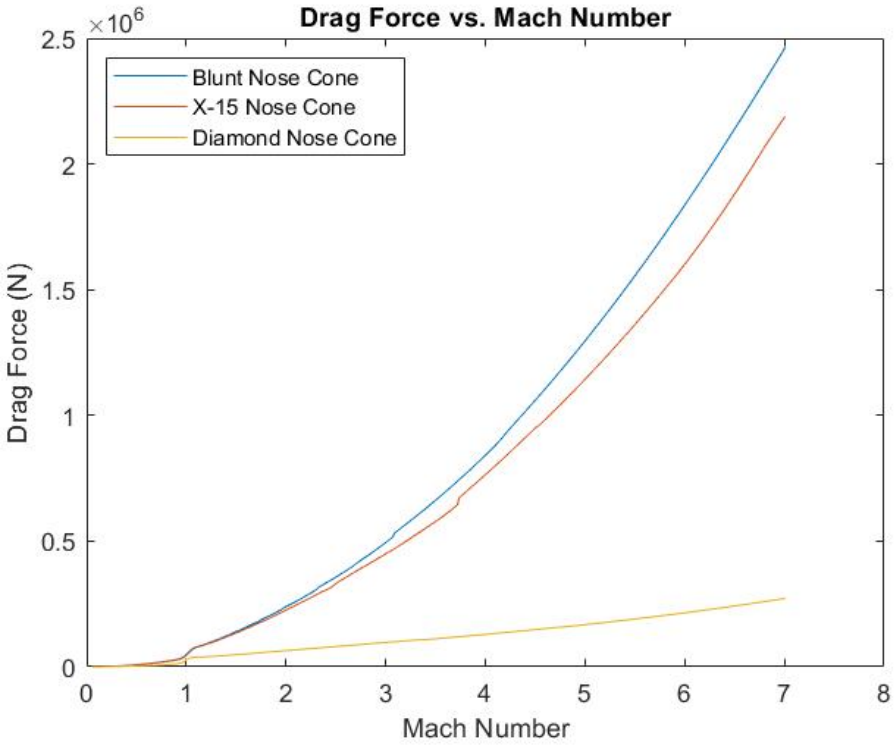

Figure 16: Drag vs. Mach number for all three geometries.

The stagnation temperature for the blunt and X-15 nose cones follow almost identical trends as the Mach number is increased. All three follow very similar profiles to their drag with the diamond

nose cone experiencing much lower temperatures than the other two. The blunt and X-15 nose cone likely follow the same stagnation temperature trend because the blunt nose cone experiences a greater drag force but also a greater surface area for the heating to spread over.

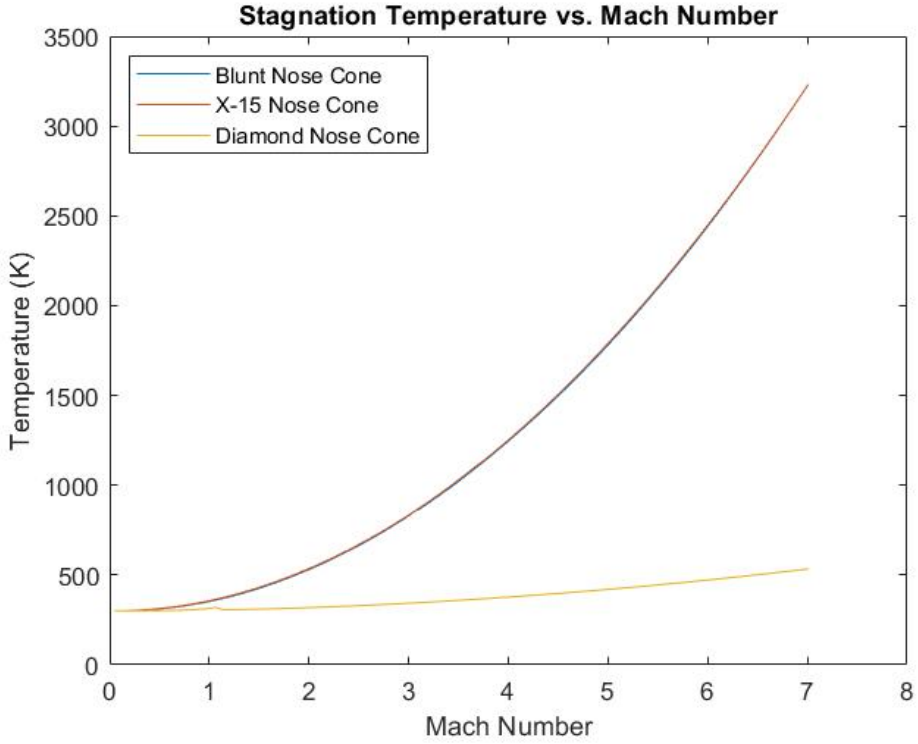

Figure 17: Stagnation temperature vs. Mach number for all three geometries.

The stagnation pressure of the blunt nose cone is the greatest because of its short vertical section creating the greatest local turning angle of the three geometries and in turn, a bow shock. The diamond nose cone experiences very low stagnation pressure in comparison because the shock is attached during supersonic flow. These results can be seen below in Figure 18.

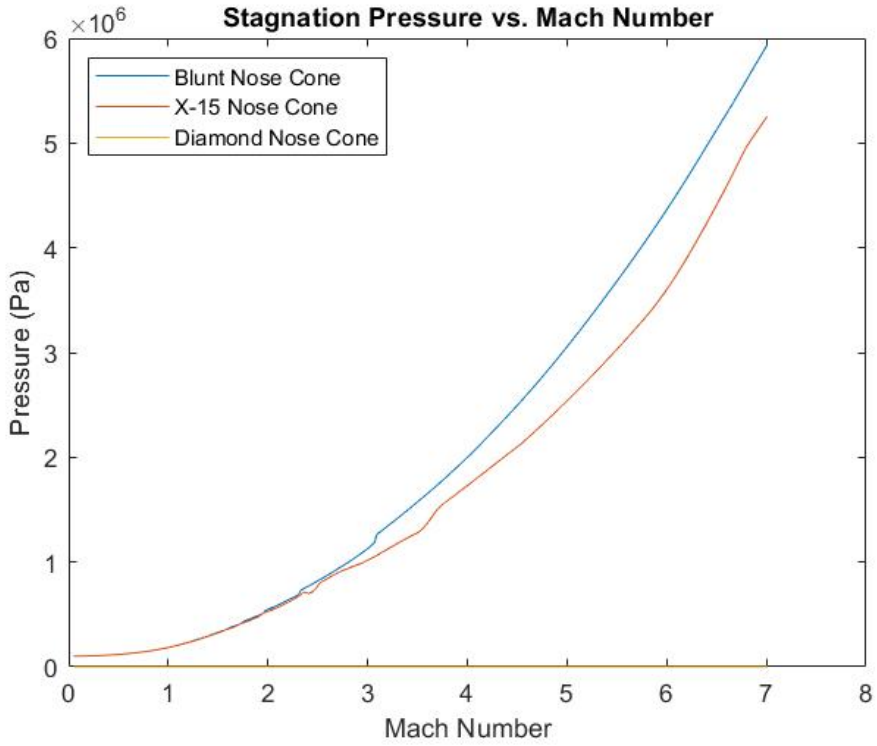

Figure 18: Stagnation pressure vs. Mach number for all three geometries.

The downstream temperature was taken at the surface of each solid 3 cm from the stagnation point. The blunt nose cone experiences much greater temperatures at this location than the other two profiles because the blunt tip provides a greater surface area that is heated on the leading edge. As seen previously, this greater surface area leads to a higher drag, resulting in greater heating of the blunt nose further from the stagnation point. This can clearly be seen below in Figure 19.

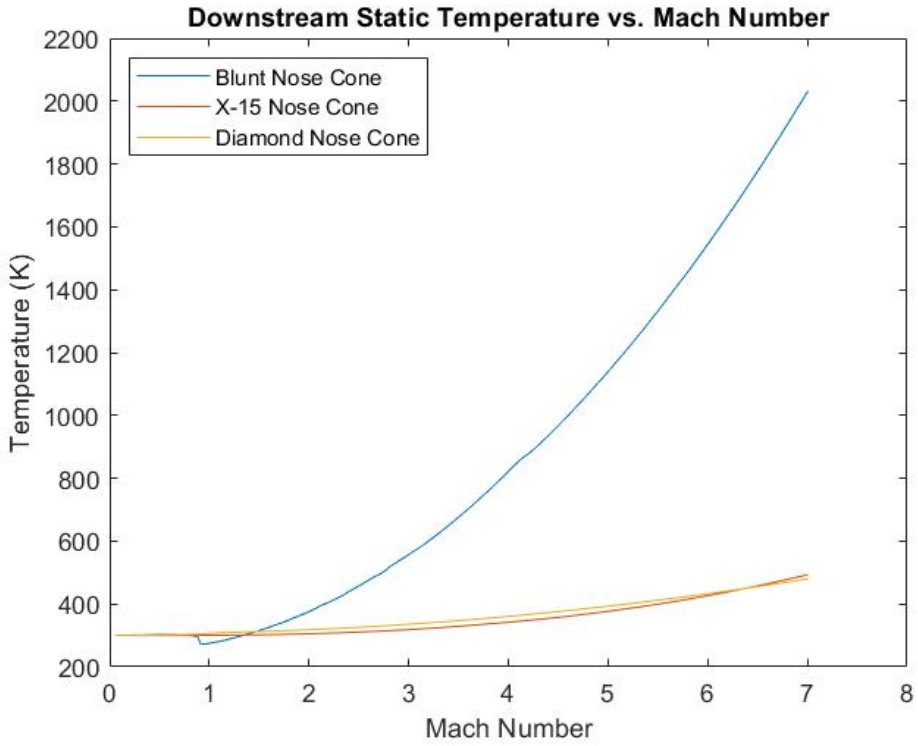

Figure 19: Surface temperature 3 cm from stagnation point vs. Mach number for all three geometries.

The heat flux from the fluid into all walls of the solid can be seen below in Figure 20. All three follow a similar trend with the blunt nose cone experiencing the greatest heat flux. This is because the blunt nose cone provides the greatest flow obstruction, creating the most heat generation in the flow-solid interface.

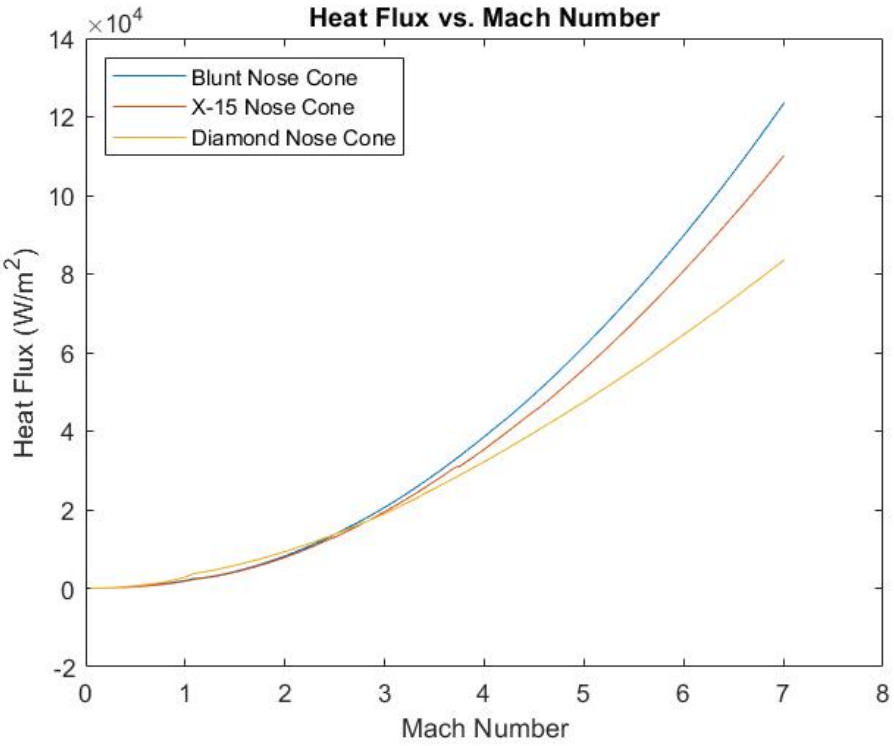

Figure 20: Heat flux into solid vs. Mach number for all three geometries.

Below, in Figure 21, is an example of a temperature contour of the blunt nose cone after 17.35 seconds of flow ramping up in Mach number. This contour represents the behavior of the two other geometries as well.

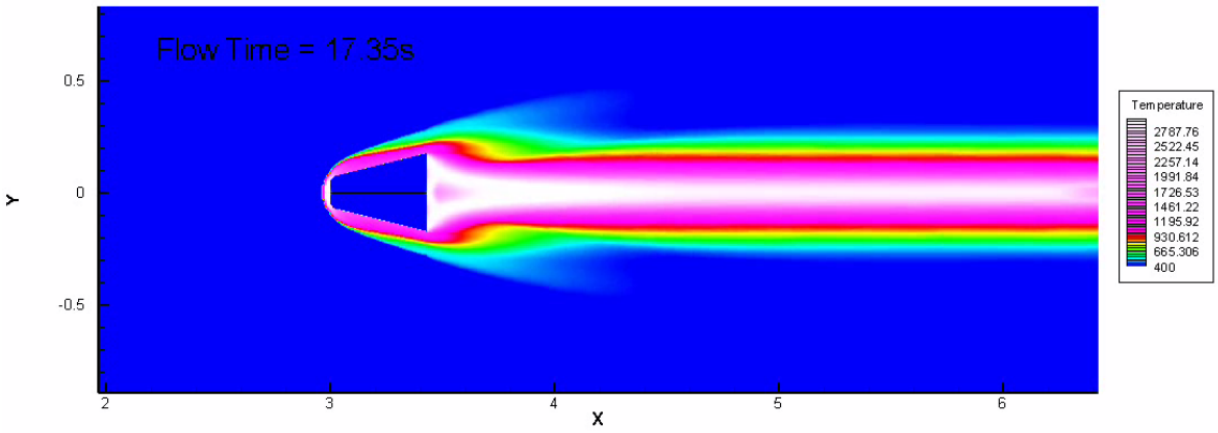

Figure 21: Temperature contour of the blunt nose cone geometry at a flow time of 17.35 seconds.

7.2 Constant Mach Number

At a constant Mach number of 6.04, the X-15 nose cone experienced the greatest stagnation temperatures. The blunt nose cone has a greater area for thermal energy to diffuse through resulting in lower stagnation temperatures during supersonic flow when compared to the X-15 nose cone. The diamond profile reaches a steady state solution almost immediately and the other two nose cones also appear to be approaching a steady state solution after 150 seconds.

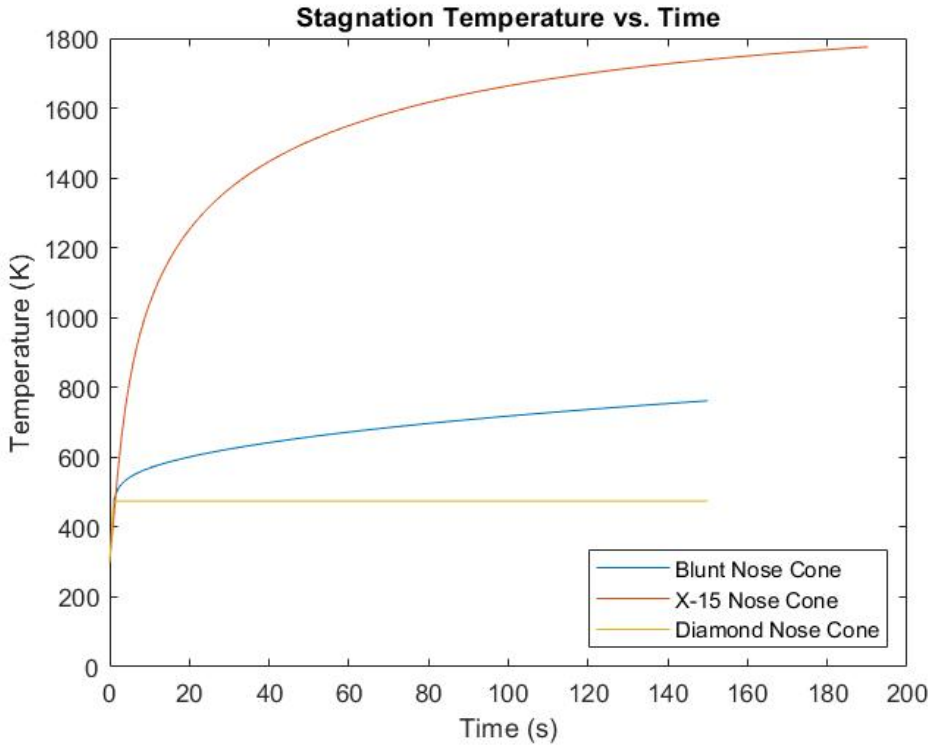

Figure 22: Stagnation temperature vs. time for all three geometries at a constant Mach number of 6.04.

The downstream location mentioned previously was examined again for the constant Mach case. It was found that the diamond nose cone reaches a steady state temperature in this location within 10 seconds. The X-15 nose cone had not yet reached a steady state at about 190 seconds but appears to be approaching one as the slope of the curve is decreasing. The blunt shaped nose cone experiences greater temperatures than the other two shapes, which, as previously stated, can be expected because of the greater temperature distribution and thermal energy absorption.

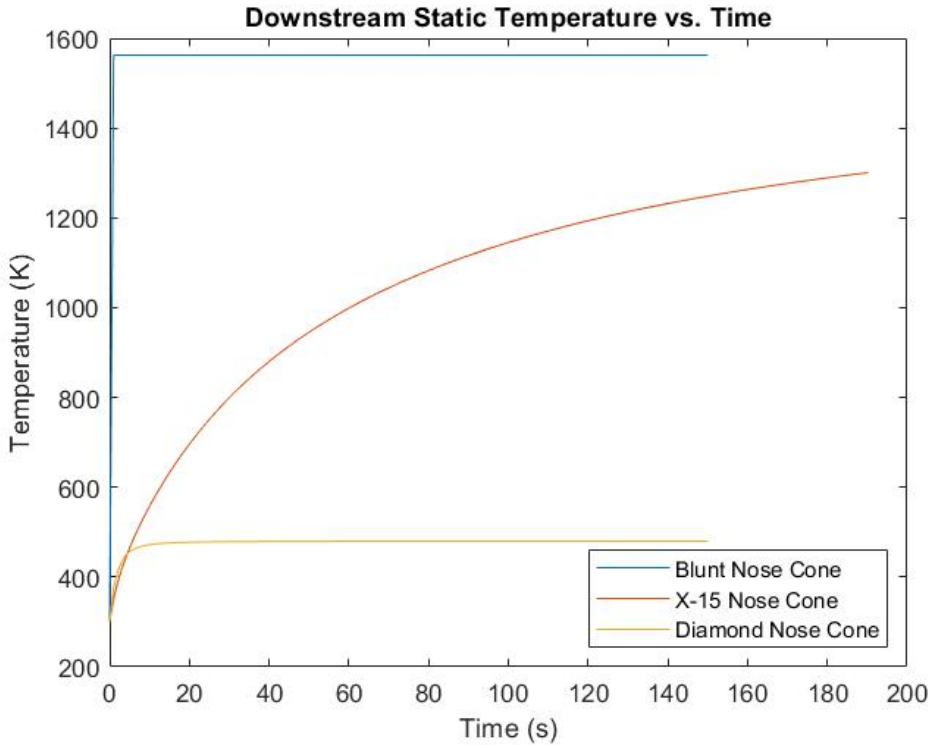

Figure 23: Downstream temperature vs. time for all three geometries at a constant Mach number of 6.04.

The heat flux into the solid begins at a maximum for each shape and starts to decrease. This is because the temperature differential between the surface of the solid and the fluid is decreasing as time increases. The blunt nose cone experiences the largest heat flux and the slowest decrease because it has the largest volume to diffuse the heat through. Each of the geometries are beginning to asymptote to a constant value, or a steady state.

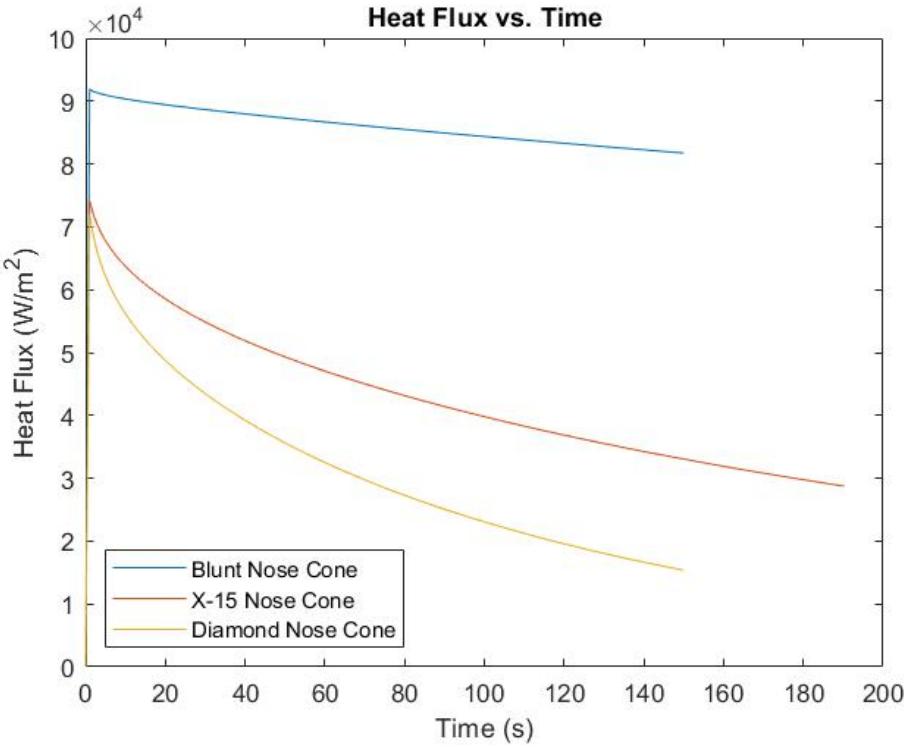

Figure 24: Heat flux into solid vs. time for all three geometries at a constant Mach number of 6.04.

Below, the temperature contours for Mach 6.04 flow after 93 seconds for the blunt nose cone can be seen in Figure 25. The diffusion of heat across the solid body can be clearly observed. The characteristics portrayed by this contour are representative of all three geometries.

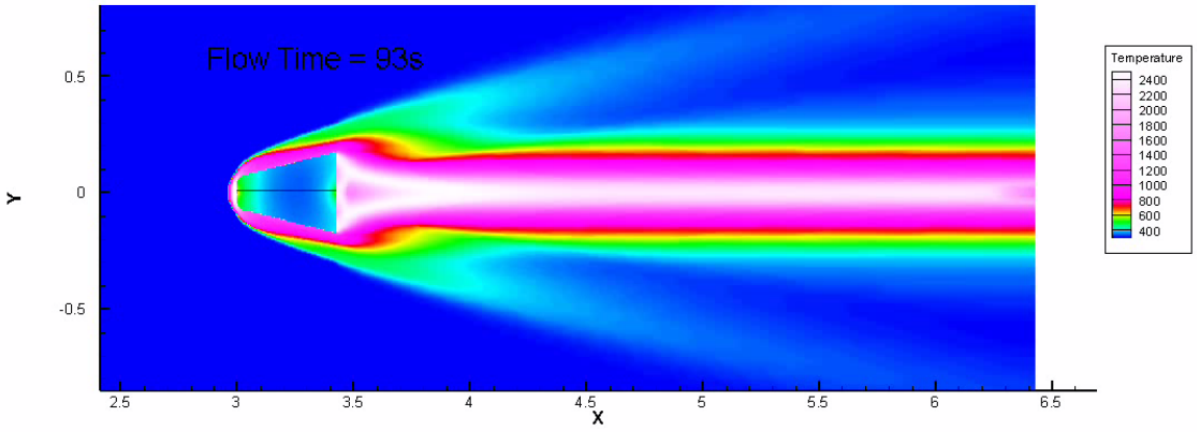

Figure 25: Temperature contour of the blunt nose cone geometry after 93 seconds of flow at Mach 6.04.

Data recorded by the X-15 in testing resulted in a maximum stagnation temperature of about 870 degrees kelvin during a flight where a Mach number of 6.04 was reached [4]. For the model X-15 nose cone, the ramp up Mach number simulation resulted in a stagnation temperature of about 2250 kelvin at a Mach number of 6. The constant Mach simulation resulted in a maximum stagnation temperature of just under 1800 kelvin after 190 seconds at Mach 6.04. The large temperature differentiation between the simulated data and the actual recorded data are the cause of a few factors that were listed in the assumptions previously.

8 Conclusions

It is apparent from the results of the simulations that there is a difference between the three different shapes in terms of thermal characteristics. For the ramp up Mach scenario, the blunt nose had the highest drag and the diamond showed the lowest drag overall. The values were very similar in the subsonic regime but diverged in the supersonic and hypersonic regime. The stagnation temperature was very similar for the blunt nose and X-15 nose shapes, whereas the diamond nose had overall a much lower stagnation point temperature throughout the ramp up period. The downstream static temperature at 0.03 meters behind the stagnation point was similar for the diamond and X-15 shape, but much higher for the blunt nose shape, likely because 0.03 meters was still on a fairly vertical portion of the blunt model but on a more angled portion of the other models. The heat flux was similar for all three models but was highest for the blunt nose shape and lowest for the diamond shape. For all of the cases the data exhibited exponential growth.

For the constant Mach number case, the stagnation point temperature was highest for the X-15 shape and lowest for the diamond shape, whereas the static temperature on the surface 0.03 meters behind the stagnation point was highest for the blunt nose shape and lowest for the diamond shape. The heat flux was highest for the blunt nose shape and the diamond heat flux was lowest. All of the data for the constant case exhibited asymptotic behavior.

Overall, the results of these simulations show that at hypersonic speeds, the blunt nose cone experiences a lower stagnation temperature than the X-15 nose cone model, likely because it has more surface area and volume to distribute heat. The drag was higher for the blunt shape and X-15 shape in the ramp up case so it is not surprising that the temperature is higher for the non-diamond cases. However, the heat distribution is better overall for the blunt shapes therefore they are a better option for higher Mach cases with respect to temperature.

References

[1] Anderson, John D. Modern Compressible Flow: With Historical Perspective. 3rd ed., McGraw-Hill Education, 2012.

[2] Engineering ToolBox, (2003). Conductive Heat Transfer. [online] Available at: https://www.engineeringtoolbox.com/conductive-heat-transfer-d_428.html

[3] Engineering ToolBox, (2003). Convective Heat Transfer. [online] Available at: https://www.engineeringtoolbox.com/convective-heat-transfer-d_430.html.

[4] Kordes, Eldon E., et al. Structural Heating Experiences on the X-15 Airplane. Armed Services Technical Information Agency, 2014, Structural Heating Experiences on the X-15 Airplane.

[5] Shpilrain, E E. "AIR (PROPERTIES OF)." THERMOPEDIA, 2 Feb. 2011, www.thermopedia.com/content/553/.

[6] "Special Metals INCONEL® Alloy X-750." ASM Aerospace Specification Metals Inc., asm.matweb.com/search/SpecificMaterial.asp?bassnum=NINC35.

[7] X-15 Status Report, Paul F. Bikle/FRC to J. Martin/NASA Headquarters, 4 November 1968, pp. 1-2. In the files at the DFRC History Office.

[8] Young, A. D. "The Calculation of the Total and Skin Friction Drags of Bodies of Revolution at Zero Incidence." R.A.E, 1939.